Title: Automatic Extraction and Analysis of Ice Layering in Radar Sounder Data

This paper appears in: IEEE Transactions on Geoscience and Remote Sensing

Date of Publication: 2013

Author(s): Adamo Ferro, Lorenzo Bruzzone

Volume:51, Issue: 3

Page(s): 1622-1634.

DOI: 10.1109/TGRS.2012.2206078

Automatic Extraction and Analysis of Ice Layering in Radar Sounder Data

Adamo Ferro, Lorenzo Bruzzone, *Fellow, IEEE*

***Abstract*—Nowadays, the interest on the development of orbiting radar sounders for the observation of Earth polar areas is increasing. In this context, the analysis of the structure of the ice stratigraphy is of primary importance for the study of the past history and for the prediction of the evolution of icy environments. However, as proven by planetary missions, orbiting radar sounders provide a huge amount of data. Thus, the development of automatic techniques for the analysis of these data is of fundamental importance for a proper data exploitation. In this paper we propose a novel method for the automatic detection of subsurface linear features from radar sounder data acquired in icy regions showing extended layering. The proposed method allows the estimation of the position of the linear features with sub-pixel accuracy. Moreover, each detected linear interface is treated as a single object which is completely described by the position of its points, the estimated local width and the contrast. This allows the direct measurement of geometrical and radiometric parameters (e.g., slope angle, intensity) without the need of further post-processing steps. The paper also proposes some measurements for deriving from the output of the proposed technique important variables that can characterize quantitatively the properties of the detected linear features (e.g., mean depth, mean intensity) and their distribution (e.g., number and density of layers). The effectiveness of the proposed method is confirmed by the results obtained on several radargrams acquired by the Shallow Radar (SHARAD) on the North Pole of Mars.**

I. Introduction

RADAR sounding is a well known nonintrusive technique which allows the investigation of the structural and dielectric characteristics of the subsurface. This is performed by transmitting waves in the MF, HF or VHF frequency ranges into the subsurface and recording the signals scattered back from subsurface structures or dielectric discontinuities [1]. Radar sounder data are usually stored as radargrams. Radargrams are 2D images that represent the recorded echo power for a given range position as a function of time on one axis, and as a function of the instrument along-track position on the other. Therefore, a radargram shows a sounding profile taken over a certain ground track.

Radar sounders are often mounted on flying platforms, such as airplanes or satellites. The former are widely used for the study of Earth's poles and can provide local or regional mapping on areas of interest [2]. Although interest has been shown by the glaciological community for an Earth orbiting sounder [3], at the time of writing spaceborne radar sounders have been used only for the exploration of other planets or moons. Examples are the Lunar Radar Sounder (LRS) of the Japanese orbiter Kaguya [4], the Mars Advanced Radar for Subsurface and Ionosphere Sounding (MARSIS) on the ESA's Mars Express orbiter [5], and the Shallow Radar (SHARAD) of the Mars Reconnaissance Orbiter of NASA [6]. The latter two instruments are currently operating at Mars and are providing high quality data which make it possible a detailed study of the subsurface of the Red Planet. In particular, the SHARAD instrument has the capability to produce radargrams with a vertical (range) resolution of about 10 m in ice. This makes it possible to reveal the ice stratigraphy of Mars' poles [7], [8], and to detect fine linear interfaces in other areas of the planet [9]. New planetary radar sounder instruments are planned to be included in future missions devoted to the study of other bodies, such as the moons of Jupiter [10] and Titan [11]. Activities for the definition of an Earth orbiting sounder are also in progress.

One of the most important applications of radar sounders is the analysis of the subsurface in icy regions (e.g., Greenland, Antarctica, poles of Mars). Indeed, ice is one of the most transparent materials at the aforementioned frequencies, thus making the penetration of the signals into the subsurface feasible even for several kilometers [12]. A salient characteristics of icy regions is the presence of extended layering due to the deposition and subsequent solidification of snow in different periods. The study of the structure of the ice stratigraphy (e.g., position and density of the ice layers) is very important for many reasons. Primarily, the analysis of the ice stratigraphy allows the estimation of ice age and accumulation rate, and is necessary for constraining ice flow models [13], [14]. All the aforementioned factors are key parameters for the study of the past history and for the prediction of the evolution of icy environments. Focusing on the Earth, nowadays this is of primary importance in the framework of the assessment of the impact of climate changes on the Earth's system.

Orbiting radar sounders provide a huge amount of data. In the case of planetary missions, the analysis of such data has been carried out mainly by means of manual investigations. This limits their return, as manual analysis are time consuming and inherently subjective. This calls for the development of automatic or semi-automatic techniques for the analysis of radar sounder data that can extract relevant information from radargrams in an efficient and fast way. Such techniques can thus help the scientific community in the selection of interesting radargrams, in the detection and characterization of subsurface features, in the correlation of such features between large sets of radargrams taken on adjacent tracks, and in global mapping.

The development of techniques for the automatic analysis

A. Ferro and L. Bruzzone are with the Department of Information Engineering and Computer Science, University of Trento, Via Sommarive 5, I-38123, Trento, Italy, e-mail: adamo.ferro@disi.unitn.it, lorenzo.bruzzone@ing.unitn.it.

Manuscript received Month day, year; revised Month day, year.

of radar sounder data has not been addressed sufficiently in the literature. In [15] we made a first step towards the automatic analysis of planetary radar sounder signals by presenting a statistical analysis of the signals and proposing a technique for the automatic detection of polar basal returns. As mentioned previously, subsurface layering is another important characteristic. In this paper we thus focus on the automatic detection and characterization of subsurface linear features in sounding profiles of regions showing extended layering. Related works are mainly devoted to the automatic analysis of data acquired by surface-mounted ground penetrating radars (GPR) showing linear and hyperbolic returns [16]–[20]. Linear features are often detected by means of the Hough transform or modeled as the limit of hyperbolas with no slope. These approaches are suited for GPR radargrams containing clear straight lines, but they are not appropriate for radar sounder data in which linear features are not straight and change slope locally. In fact, radar sounder radargrams cover a much longer track than GPR acquisitions usually with a much worse along-track sampling, thereby showing the large scale shape of subsurface linear interfaces (e.g., due to topography). To our knowledge, the only attempt to the automatic detection of shallow linear features in radar sounder data reported in the literature was made by Freeman *et al.* [21] using SHARAD radargrams. In their work the authors used a combination of image filterings followed by a threshold operation. The goal of the filterings is: i) to reduce background noise, ii) to normalize the data using a band-pass Gaussian filter; and iii) to highlight almost-horizontal linear features by means of a matched filter. Indeed, the algorithm relies on the assumption that linear features have very low slopes. In order to achieve this, a coordinate transformation is applied in order to flatten the surface topography, and thus reduce the induced layer slopes prior to image filterings. The output of the processing is a binary image where the pixels belonging to linear interfaces are highlighted. Therefore, the method does not detect directly single linear features and needs further processing steps in order to extract detailed information on their radiometric and geometrical characteristics.

In this paper we propose a novel technique for the automatic detection of subsurface linear features in layered media which allows the direct estimation of the position of the single linear features with sub-pixel accuracy. The method does not rely on specific geometrical assumptions (e.g., flatness of subsurface features). Moreover, each detected linear interface is treated as a vector object which is completely described by the position of its points, and its estimated local width and contrast, thus allowing the direct measurement of geometrical or radiometric parameters (e.g., slope angle, intensity) without the need of further post-processing steps (as necessary for simpler techniques based on image filtering and thresholding). The paper also proposes some measurements for deriving from the output of the proposed technique variables that characterize quantitatively the properties of the detected linear features (mean depth, mean intensity, relative mean contrast) and their distribution (number of features, density of layers). Despite that the proposed technique is general, in this paper we evaluate its effectiveness by considering SHARAD radargrams

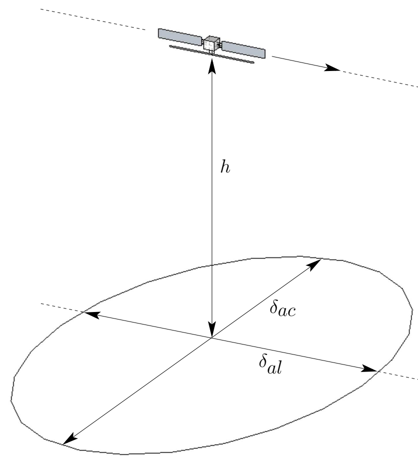

Fig. 1. Acquisition geometry of a radar sounder instrument. h is the platform height, δ_{al} and δ_{ac} are the along- and across-track resolutions on ground, respectively.

of the North Pole Layered Deposits (NPLD) of Mars. The results show the effectiveness of the proposed method.

The remainder of the paper is organized as follows. Sec. II describes briefly the acquisition geometry of a radar sounder and defines the notation used throughout the paper. Sec. III presents the proposed method for the automatic detection of linear features in radar sounder radargrams. Sec. IV shows the experimental results obtained on real SHARAD radargrams of the NPLD of Mars. Finally, Sec. V draws the conclusions of the paper and suggests future developments.

II. Reference System and Notation

In this section we fix the reference system and define the notation used throughout the paper.

A. Radargram Reference System

The acquisition geometry of a radar sounder instrument is depicted in Fig. 1. The platform on which the instrument is mounted flies at a certain altitude h over the ground. Such an altitude can span between several hundreds of meters and several hundreds of kilometers, depending on the type of platform (i.e., airplane or satellite). The resolution on ground of the system depends on the type of antennas and on the signal processing techniques adopted. In general, the spatial resolution in the along-track direction δ_{al} can be sharpened by synthetic aperture processing [1]. In contrast, the resolution in the across-track direction δ_{ac} is usually linked to the real antenna aperture and the surface roughness. This may lead to a wide swath in the across-track direction, which can be of some tens of kilometers for a spaceborne radar sounder [5], [10]. When relevant topography is present within the ground swath, lateral echoes coming from the surface can appear in the range corresponding to the subsurface. Such returns become relevant on irregular (sloped) or rough surfaces, and their strength depends on the system spatial resolution and on the relation between the radar wavelength and the size of the surface irregularities. The presence of such echoes represents one of the main factors which complicate the development and reduce the effectiveness of automatic techniques for the analysis of radar sounder data. Indeed, they can be erroneously detected as (or mask) actual subsurface features.

In this paper radar sounder radargrams are considered as 2D images where each pixel at the position (x,y) corresponds to a power sample acquired by the instrument at a given along-track position (corresponding to the column index x) and at a certain time (corresponding to the row index y). The sequence of samples belonging to a certain column x of the radargram is also referred to as *echo* or *frame*. Fig. 2 shows schematically the defined reference system. The geographical position of the track on ground can be reconstructed by means of ancillary information usually distributed with the radargrams. In contrast, the vertical range of the samples can be known exactly only in the time domain. Indeed, in order to translate the sample positions from time to depth it is necessary to assume a certain dielectric constant $\varepsilon_{\mathrm{SS}}$ for the subsurface [1].

B. Definition of Linear Feature

A generic linear feature λ_i in a radargram acquired on a icy region will be described as a set of four-element tuples as follows:

$$\begin{aligned}\lambda_i = \{&(x,y,w,c) : (x,y) \in \Phi_i \\ &\wedge\ w = \Omega_{\lambda_i}(x,y)\ \wedge\ c = C_{\lambda_i}(x,y)\}\end{aligned} \tag{1}$$

where Φ_i is the representation of λ_i in the image reference system, and Ω_{λ_i} and C_{λ_i} are operators which calculate the local width and contrast of λ_i at a given point (x,y), respectively. The line contrast is defined as the difference between the line intensity and its surrounding, assuming the simplifying assumption that each line section has a rectangular shape. Note that Φ_i includes only the skeleton of a linear feature, and does not provide any information on its thickness. We define as Φ_i^w the set of pixels corresponding to the area of the radargram that is described by the region having as axis the points $(x,y) \in \Phi_i$ and a local width defined for each point as $w = \Omega_{\lambda_i}(x,y)$. Fig. 2 shows graphically the definitions given in this paragraph.

It is worth noting that the definition of λ_i allows one to calculate for each linear feature a set of derived measures which can be computed also locally by selecting a subset of the elements composing λ_i (e.g., line total length, mean width, local mean contrast). For the analysis of actual subsurface reflections, such measures can be then straightforwardly translated in physical quantities (e.g., geographical length of a linear interface, mean intensity of the reflection). In order to give the most general definition, in this paper we will use as unit for linear feature width and length the number of pixels of the radargrams. In fact, radargrams of different sensors have different resolutions, both in range and along-track. Moreover, even radargrams from the same instrument can be focused at different resolutions. Therefore, the relation between the physical length and width of a reflection and their representations in the image domain are not unique. Using physical quantities for the definition of the parameters of the proposed technique would be thus not general, but linked to a certain instrument and focusing approach.

III. Automatic Detection and Characterization of Linear Features in Radar Sounder Data

In this section we describe the proposed automatic technique for the detection and characterization of linear features in radar sounder data. The proposed method is a four-step procedure made up of: i) radargram denoising and enhancement, ii) line detection, iii) removal of first returns, and iv) extraction of measures of interest. Fig. 3 shows a block scheme of the proposed method. In the following we describe in detail each step of the algorithm and propose examples of derived measurements that can be calculated after the detection.

A. Radargram Denoising and Enhancement

The goal of this step is to reduce the background noise of the radargrams and enhance the signature of linear features. Noise reduction and line enhancement are performed jointly by exploiting the intrinsic correlation that linear features show on adjacent frames. As an example, a linear feature covering several adjacent frames is expected to appear at adjacent y positions. This holds independently from its intensity. A linear feature characterized by low intensity can thus be masked by noise peaks in some echoes. However, as noise is uncorrelated among the different frames, the linear feature can be preserved whereas noise is reduced. To this end, we propose for the joint radargram denoising and linear feature enhancement the use of the BM3D filter developed by Dabov *et al.* [22]. Fig. 4 summarizes the operations performed by the filter. The first step is aimed at producing a so-called basic estimate of the true image (i.e., the image with no noise). This is done by operating in a non-local way. The filter searches the radargram space for similar parcels by means of a block-matching procedure based on a square sliding window. The retrieved blocks are then stacked together to form a 3D group, which is filtered by means of hard-thresholding operated on the coefficients of a 3D transform applied to the group (for instance based on Discrete Cosine Transform or Walsh-Hadamard). The inverse 3D transform is then applied to the thresholded coefficients. Finally, the output block estimates are aggregated together using weights calculated from the thresholded coefficients. Thus, at the end of the first step a basic estimate of the denoised image is produced. Such image is used as input to the second step. In the second step, the filter performs a procedure which is similar to the one of the first step. The main difference is the use of a Wiener filter which denoises the original input image using as reference the basic estimate derived in the first step. For more details on the processing performed by the filter the reader is referred to [22].

The BM3D filter has been originally developed for optical images affected by additive white Gaussian noise (AWGN), and for this type of images it represents the state of the art. The main parameter of the BM3D filter is the estimated variance of the image background AWGN noise. Other parameters tune the size of the blocks and the maximum number of blocks per group. The BM3D filter can be properly defined also for non-AWGN noise [22], [23]. It has been also used with good results for despeckling of log-transformed synthetic aperture radar (SAR) images [24].

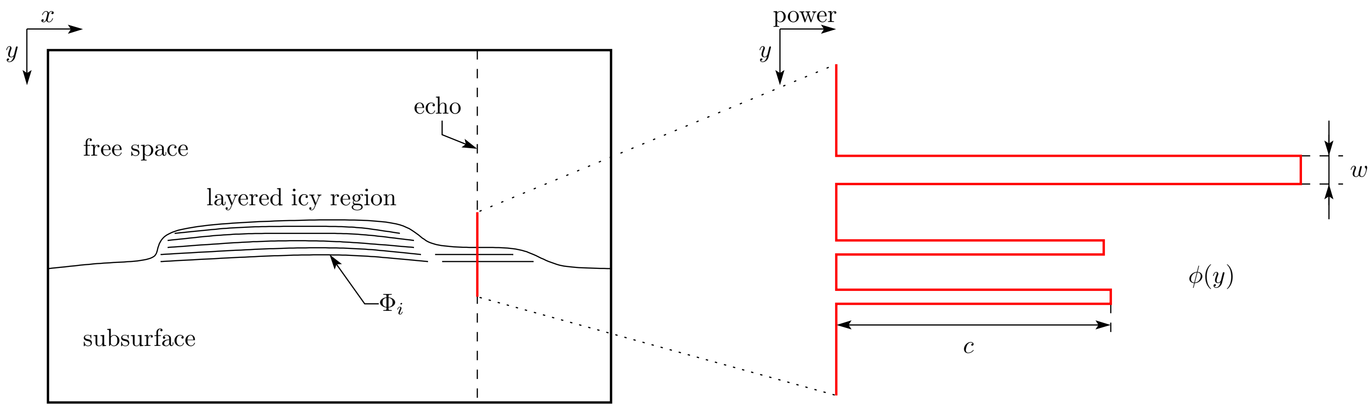

Fig. 2. Reference system and definitions of linear feature parameters as used in this paper on a simplified qualitative radargram.

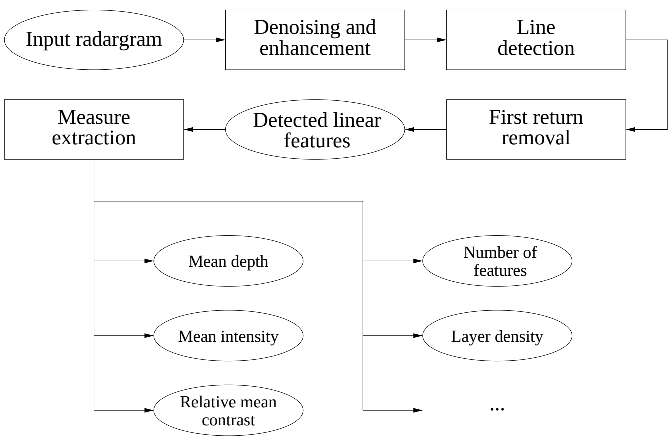

Fig. 3. Block scheme of the proposed method for the detection and characterization of linear features in radar sounder data.

In the case of radar sounder data the AWGN assumption is not valid. Noise in amplitude radargrams appears as an additive and Rayleigh distributed contribution (when no multilooking is performed) [15]. Moreover, in correspondence of any reflection, the so-called *speckle* effect appears because of the coherent nature of a radar acquisition [15], [25]. However, as it will be shown later, the use of the original BM3D filter for AWGN[1] as a step prior to line detection on stretched dB-power radargrams is very effective and sufficient for performing the subsequent line detection.

For the sake of completeness, we also point out that modified versions of the BM3D filter specifically devoted to the joint image denoising and edge sharpening have been proposed in the literature [26]. In our experiments such methods exhibited good performance. However, the edge sharpening resulted in a subsequent higher number of false line detections due to filtering artifacts. Moreover, edge sharpening changes the line intensity, making it more difficult to select the parameters of the line detector according to values directly measurable on the original radargram. For these reasons, in this paper we use the BM3D filter without edge sharpening.

[1]The implementation of the BM3D filter used in this paper is that available at http://www.cs.tut.fi/~foi/GCF-BM3D/.

B. Line Detection

In order to extract linear features from the denoised radargrams we propose to use the Steger filter [27]. The Steger filter has been originally developed for the detection of linear features in optical images and exhibited good performance also on images affected by significant noise [28]. Moreover, it has been successfully applied as a tool for primitive segmentation aimed at building detection in VHR SAR images [29], [30].

The Steger filter assumes for linear features a rectangular profile (see Fig. 2) and the detection of lines is performed by analyzing the second derivative of the convolution of such profile with a Gaussian smoothing kernel. In the 1D case (e.g., considering only a single radargram frame y), the function evaluated by the filter is:

$$\begin{aligned} r(y,s,w,c) &= g_s''(y) * \phi(y) \\ &= c\left[g_s'\left(y+\frac{w}{2}\right) - g_s'\left(y-\frac{w}{2}\right)\right] \end{aligned} \tag{2}$$

where

$$g_s(y) = \frac{1}{\sqrt{2\pi}s} e^{-\frac{y^2}{2s^2}} \tag{3}$$

is the Gaussian convolution kernel. $g_s'(y)$ and $g_s''(y)$ are its first and second derivatives, respectively, and $\phi(y)$ is the line representation in the 1D space (see Fig. 2). The line response to the filter is calculated as $|r(0,s,w,c)|$, given by:

$$|r(0,s,w,c)| = \frac{wc}{\sqrt{2\pi}s^3} e^{-\frac{w^2}{8s^2}} \tag{4}$$

According to [27], the value of s should belong to the range $\left[\frac{w}{2\sqrt{3}}, \frac{w}{2}\right]$. However, the maximum line response is obtained using the minimum value allowed for s, which is $s = \frac{w}{2\sqrt{3}}$. Therefore, in our experiments we will use this value for s. As an example, Fig. 5 shows the value of $|r(0,s,w,c)|$ for the case $w=1$ and $c=1$ with s spanning its domain range.

The mathematical description of the filter allows the unbiased calculation of the line position with sub-pixel accuracy also in the case in which the line has background with asymmetric intensities on its sides. This is important as it allows a precise estimation of the position of the linear feature independently on the fixed pixel spacing. Moreover, width and contrast can be estimated locally for each detected linear feature λ_i by properly defined Ω_{λ_i} and C_{λ_i} operators [27].

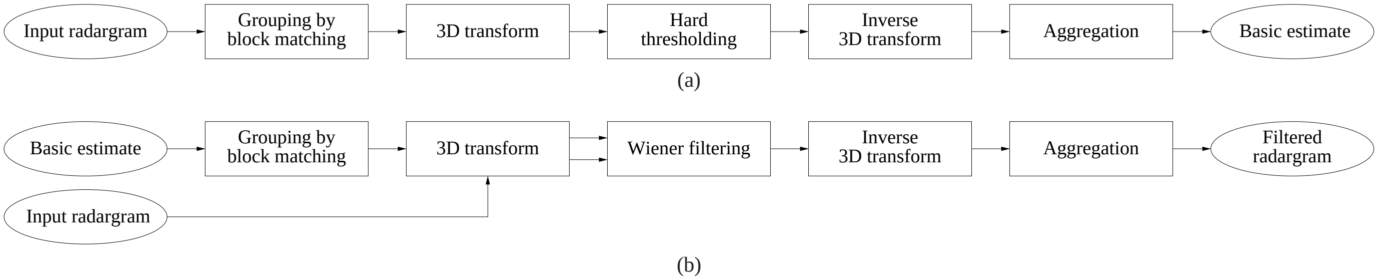

Fig. 4. Block scheme of the BM3D filter: (a) generation of the basic estimate, (b) generation of the filtered image through Wiener filtering (scheme adapted from [22]).

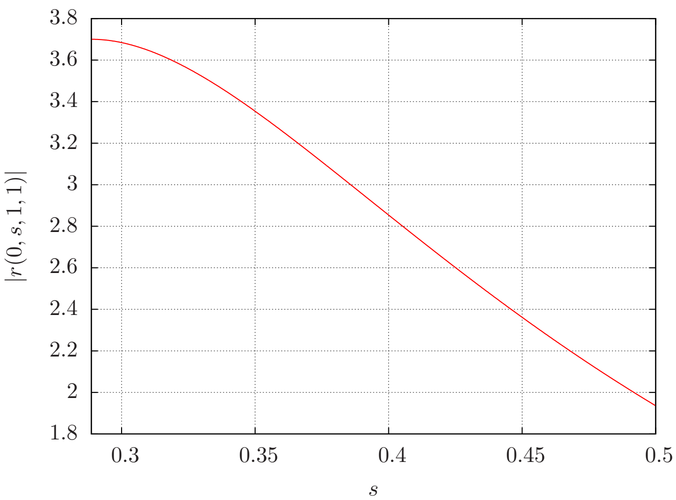

Fig. 5. Value of $|r(0, s, w, c)|$ calculated using $w = 1$ and $c = 1$, and by varying s in the range $\left[\frac{w}{2\sqrt{3}}, \frac{w}{2}\right]$.

For a given w (and thus s), the main parameter of the Steger filter which has to be set is r_{up}. r_{up} is the minimum response to the filter that triggers the detection of a line point. The algorithm also includes the possibility to link the detected line points into lines. This is performed by searching the neighborhood of line points and adding new points which have a second derivative greater than a third parameter r_{low}. The choice of r_{up} can be made by calculating the response of an ideal rect-shaped line with given width w and contrast c_{up} using (4) and choosing $s = \frac{w}{2\sqrt{3}}$. This results in:

$$r_{\text{up}} = 24\sqrt{\frac{3}{2\pi}}\frac{e^{-\frac{3}{2}}}{w^2}c_{\text{up}} \quad (5)$$

Similarly, the value of r_{low} can be calculated using in (5) a value c_{low} which represents the minimum contrast allowed for the linking of the detected line points.

C. First Return Removal

The output of the previous step is a set Λ of detected linear features λ_i. As the line detector has been applied to the whole radargram, Λ contains linear features which are caused by both surface and subsurface reflections. Therefore, in this step the algorithm removes the linear features corresponding to the first returns and preserves only the lines which are likely to belong to the subsurface. The detection of the first returns is carried out by means of the algorithm proposed in [15]. Such an algorithm detects for each frame x the position of the first sample which is statistically different from the frame background noise (which is modeled with a Rayleigh distribution). A smoothing function is then applied to the results to mitigate the effect of outliers. Note that in this step only the surface reflections appearing as first returns in the radargrams are removed. Surface clutter reflections appearing at the same range of the subsurface cannot be detected straightforwardly. Usually, this detection is accomplished by manually matching radargrams with clutter simulations [31]. Recently, this problem has been also addressed by means of an automatic technique [32]. The automatic detection of linear features in the subsurface range due to surface clutter thus involves a complex procedure which deviates from the scope of this paper. However, the development of such post-processing step will be subject of future work.

D. Extraction of Measures of Interest

As described in the previous subsections, the output of the proposed method is a set of detected linear features described as defined in (1). This description already provides useful information, such as the linear feature position, thickness and contrast. As an example, the contrast can be analyzed to extract from the detected features those which have a significant intensity difference with their background. This information could be useful to detect abrupt changes in the composition of the ice, and thus it can drive the definition of dielectric models of the ice column. Further parameters associated with the detected linear features can be also estimated. Such parameters can be computed locally for each feature, or can be related to set of features covering a certain geographical area or belonging to the same depth range. For instance, measurements that can be estimated independently for each detected linear feature are the mean intensity and the mean depth. This type of parameters can be associated to a vector for each detected linear feature, i.e., by extending the definition of (1) with new values calculated by proper operators. In the following we propose a set of measurements which can be used to extrapolate further information from the detected linear features.

1) Mean depth: The mean depth of a linear feature is defined as:

$$\bar{y}_{SS}(\lambda_i) = \frac{1}{|\Phi_i|}\sum_{(x,y)\in\Phi_i} y - y_0(x) \quad (6)$$

where $y_0(x)$ is the position of the first return in the frame x, as detected by the first return detection described in the previous subsection, and the notation $|\cdot|$ indicates the cardinality of a set.

2) Mean intensity: We define the mean intensity of a linear feature in the following way:

$$\mu(\lambda_i) = \frac{1}{|\Phi_i^w|} \sum_{(x,y)\in\Phi_i^w} I(x,y) \tag{7}$$

where Φ_i^w has been defined in Sec. II-B. $I(x,y)$ is the radargram intensity at the position (x,y).

3) Relative mean contrast: The relative mean contrast $\bar{c}_r$ of a linear feature λ_i is defined as the ratio between its mean intensity and the mean intensity of its surrounding. The latter can be extracted exploiting the feature contrast, which is estimated by the line detector. This results in:

$$\bar{c}_r(\lambda_i) = \frac{\mu(\lambda_i)}{\mu(\lambda_i) - \bar{c}(\lambda_i)} \tag{8}$$

where

$$\bar{c}(\lambda_i) = \frac{1}{|\Phi_i|} \sum_{(x,y)\in\Phi_i} C_{\lambda_i}(x,y) \tag{9}$$

is the mean contrast of λ_i.

4) Number of detected features: This measure can be defined locally to a certain range of frames and samples. We define as number of detected features the value

$$N(X,Y) = |\Lambda(X,Y)| \tag{10}$$

where

$$\Lambda(X,Y) = \{\lambda_i : (x,y) \in \Phi_i \;\wedge\; \exists(x,y) : x \in X \wedge y \in Y\} \tag{11}$$

$X = [x_{\min}, x_{\max}]$ and $Y = [y_{\min}, y_{\max}]$ define the range of frames and samples to be considered, respectively. The calculation of $N(X,Y)$ can be performed by means of a sliding window approach on the whole radargram portion related to the subsurface. This gives a 2D map of the distribution of the linear features within the radargram. If the computation is performed frame-by-frame (i.e., $|X| = 1$) on the whole Y range, the output is a 1D graph describing the number of detected subsurface linear features versus the along-track direction. This information is very useful to estimate the age of the ice column, as each layer is associated with the deposition and subsequent solidification of snow in different periods [13].

5) Layer density: The layer density is defined as:

$$D(X,Y) = \frac{N(X,Y)}{|Y|} \tag{12}$$

Similarly to the case of $N(X,Y)$, $D(X,Y)$ can be computed using a sliding window approach. This measure expresses the number of linear features per sample in the range direction. The definition takes into account the intrinsic correlation that linear features show between adjacent frames. Indeed, the size of the window in the along-track direction is not used in the denominator. The result is thus a 2D map of the density of the layers in the range direction. This measurement is linked to the ice accumulation rate. Therefore, it is important for the analysis of the past history of the ice column [14].

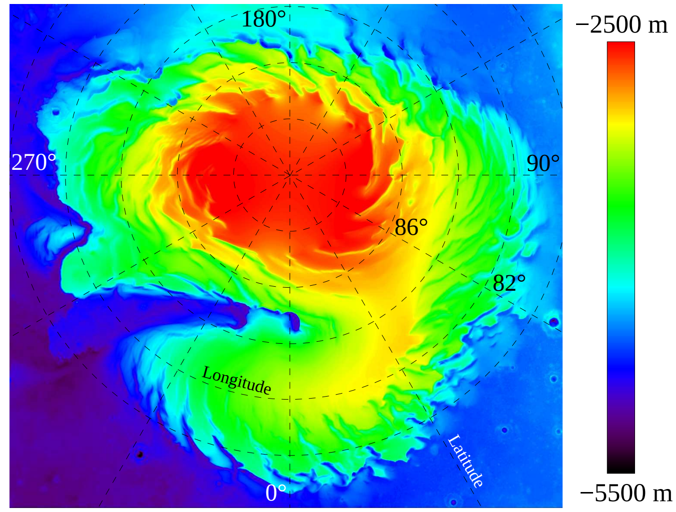

Fig. 6. Digital elevation model of the North Pole of Mars derived from Mars Orbiter Laser Altimeter (MOLA) [33] data.

The size of the sliding window should be determined depending on the resolution of the data and on the size of the structures that have to be highlighted. In general, large windows produce density maps with low detail but that are useful to infer the general distribution of the features. On the contrary, small windows can highlight better local feature patches at the cost of more visible blocking artifacts.

It is worth noting that mean depth, number of features, and density are defined in the radargram image space. However, they can be related to geographic and time scales by applying the appropriate conversion factors.

IV. Experimental Results

In this section we present the results obtained by the proposed technique on real radar sounder data. First, we present the dataset used in the experiments. Second, we show the output of the BM3D filter on sample radargrams and frames in order to discuss its denoising capabilities. Third, we study qualitatively the influence of the parameters of the line detector on its detection performance. Then, we measure quantitatively the detection performance of the proposed method for a fixed set of parameters. Finally, we show examples of measures extracted automatically from the radargrams.

A. Dataset Description

In order to assess the performance of the proposed technique we used many different SHARAD radargrams taken on the NPLD of Mars. Since we obtained very similar results, in the following we focus the attention (for space constraints) on four radargrams (see Fig. 7). It is worth noting that the presented method is general and can be applied to any radargram type (e.g., acquired by other radar sounders) with a proper tuning of parameters, which depend on the technical characteristics of the instrument adopted. The test radargrams refer to flat regions of the NPLD of Mars. A digital elevation model (DEM) of the NPLD is shown in Fig. 6. In the considered areas, surface clutter is very limited and this allows us to

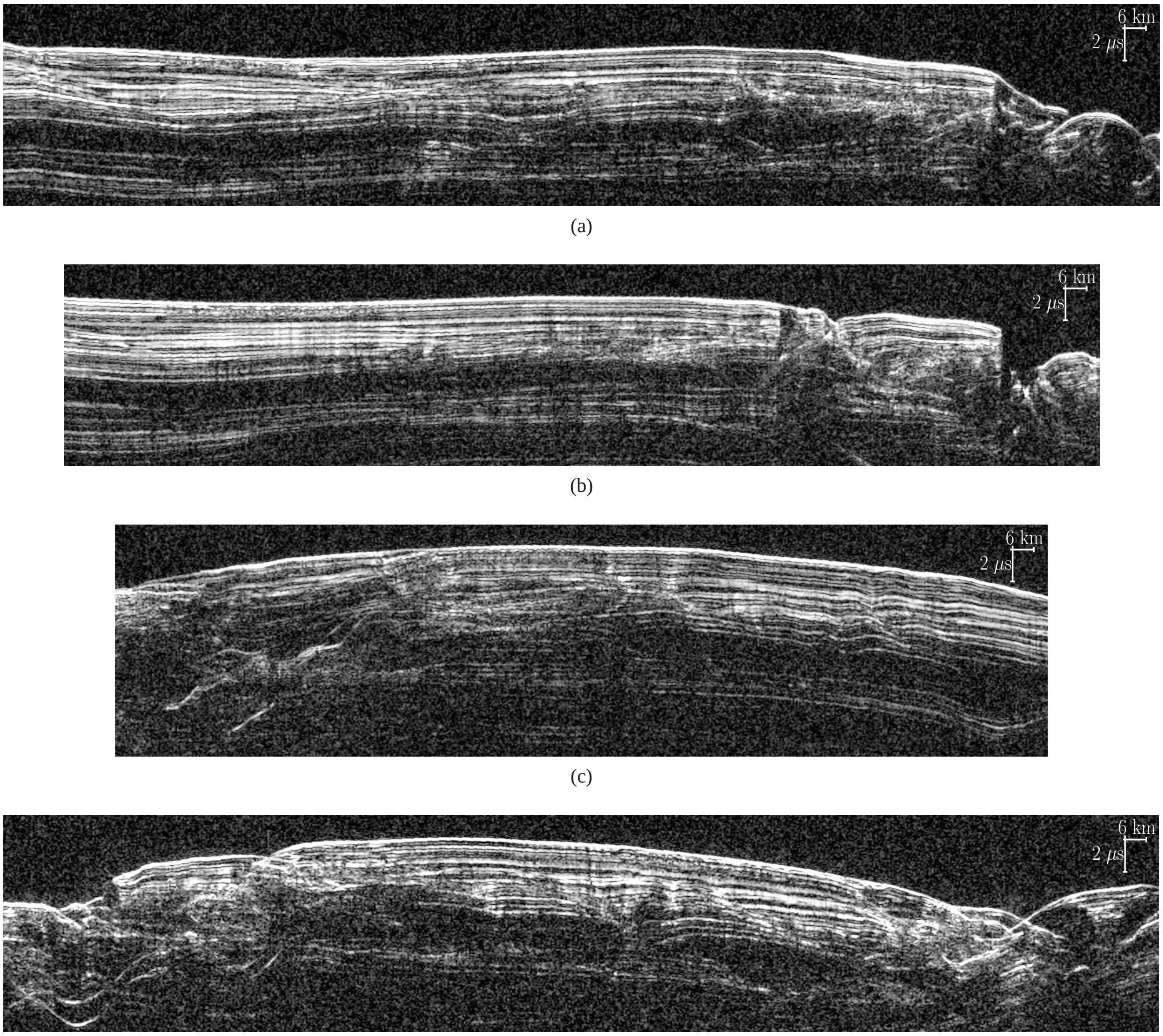

Fig. 7. SHARAD radargrams (a) 520501000, (b) 528401000, (c) 1041902000, and (d) 1591701000.

focus on the detection of actual subsurface linear features. We will consider only the upper part of the radargrams (i.e., the first 7.5-11 μs after the first detected return for each frame, depending on the considered radargram), corresponding to a densely layered shallow subsurface. The radargrams have been focused using the FPB processor [34] hosted at the Southwest Research Institute of Boulder, CO, USA. The data have been converted to dB and thresholded in the range $[\bar{n}_{\mathrm{dB}}-3, \bar{n}_{\mathrm{dB}}+32]$ dB, where $\bar{n}_{\mathrm{dB}}$ is the mean noise power measured on the radargram expressed in dB. Finally, the radargrams have been stretched in the range [0,255]. The spatial resolution of the radargrams is approximately 450 m $\times$ 3 km (along $\times$ across track) with an along-track sampling of about 115 m. The range sampling is of 37.5 ns, corresponding to 5.63 m in free space and slightly more than 3 m in an icy subsurface ($\varepsilon_{\mathrm{SS}} = 3.15$). However, as mentioned in the introduction, the range resolution of SHARAD is about 10 m in ice.

The average running time of the proposed method on the test radargrams is of less than one minute using one core of a laptop equipped with an Intel® Core$^{\mathrm{TM}}$ i5 M540 and 4 GB of RAM.

B. Radargram Denoising and Enhancement

The output of the BM3D filter for two of the test radargrams is presented in Fig. 8. The figure shows the capability of the filter to flatten the noise background while preserving, and enhancing, the linear features present in the radargrams. These effects can be appreciated more in detail in Fig. 9. The figure shows one echo taken from the test radargram of Fig. 7a before and after the application of the BM3D filter. Note that the filter mostly preserves the actual intensity value of the linear features, thus making the choice of the parameters of the line detector directly related to the intensity of the features in the original radargram. In our experiments we fixed the size of the blocks used by the BM3D filter to 32 $\times$ 32, and set the maximum number of blocks per group to 16. We obtained the best tradeoff between denoising and feature enhancing by setting the AWGN standard deviation parameter of the

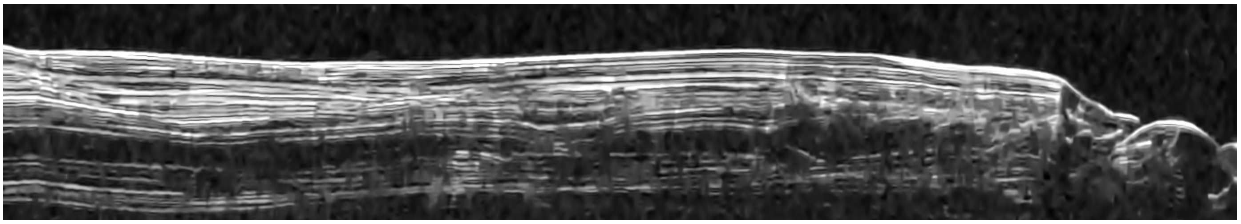

(a)

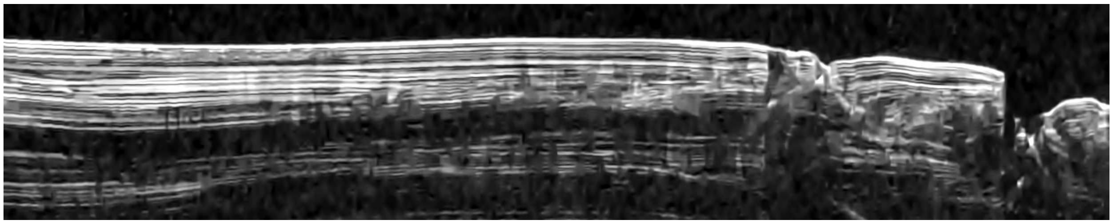

(b)

Fig. 8. SHARAD radargrams (a) 520501000 and (b) 528401000 after the application of the BM3D filter.

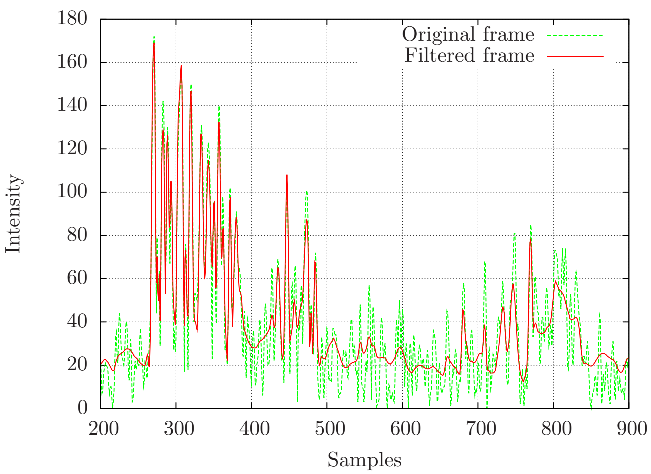

Fig. 9. Sample frames taken from the radargram of Fig. 7a before (dotted green curve) and after (solid red curve) the application of the BM3D filter.

filter equal to the background noise dynamic measured on the radargrams, which is on the order of 60 in the considered dataset.

C. Selection of the Parameters of the Line Detector

In order to select the best parameters to be used as input to the proposed technique and to understand the dependence of the results on the parameter values, we analyzed the results obtained by the method with different input parameters. In particular, we studied the dependence of the results on the choice of w and c_{up}. The value of c_{low} has been fixed to 2 for all the experiments. Lines shorter than 10 pixels have been discarded both in the reference and in the detected maps. In fact, the proposed technique is suited for the analysis of subsurface areas showing extended layering where linear interfaces usually appear for long distances. As our goal is to detect significant layers, small lines are discarded as they can be associated with other features of ice. Lines with a horizontal inclination greater than 45° have been also discarded. Such constraint comes from the fact that standard radar sounder focusing processing makes it difficult to detect returns from surfaces with high slopes. Thus, inclined features have high probability to be false alarms.

1) Dependence on w: The evaluation of the influence of w on the results obtained by the proposed technique has been carried out by applying the method using three different values (2, 4 and 6) on several test radargrams. In these experiments the value of c_{max} has been fixed to 3. On the one hand, as expected the results show that increasing w results in a lower sensitivity of the technique to thin linear features. On the other hand, linear features thicker than the selected value of w are still well detected. The number of false alarm is overall low and the detection accuracy of the algorithm is high. A slightly greater number of false alarms is associated with higher values of w. This can be explained by analyzing (5). Indeed, for a given value of c_{max} the maximum line response r_{max} decreases by increasing w, thus increasing the probability of false alarms.

2) Dependence on c_{max}: In this tests we fixed the values of w to 2. The value of c_{max} has been set to 3, 10 and 20. As expected, by increasing the value of c_{max} the proposed technique detects only the most salient lines, whereas linear features with low contrast are not detected. For the aim of this paper low contrast features are important. Therefore, low values of c_{max} will be considered in the following.

D. Quantitative Performance Analysis

The qualitative analysis presented in the previous subsection allowed us to define a range of values for the parameters of the proposed technique that permits the effective application of the method to the test dataset. In particular, the values which gave the best results are $w = 2$ and $c_{\text{max}} = 3$. Fig. 10 shows the results obtained on two of the four test radargrams. Using those parameters, in this section we thus analyze quantitatively the performance of the proposed method on the four SHARAD radargrams shown in Fig. 7. Each radargram contains a large number of lines with different lengths and widths. The amount of short/long and thin/thick

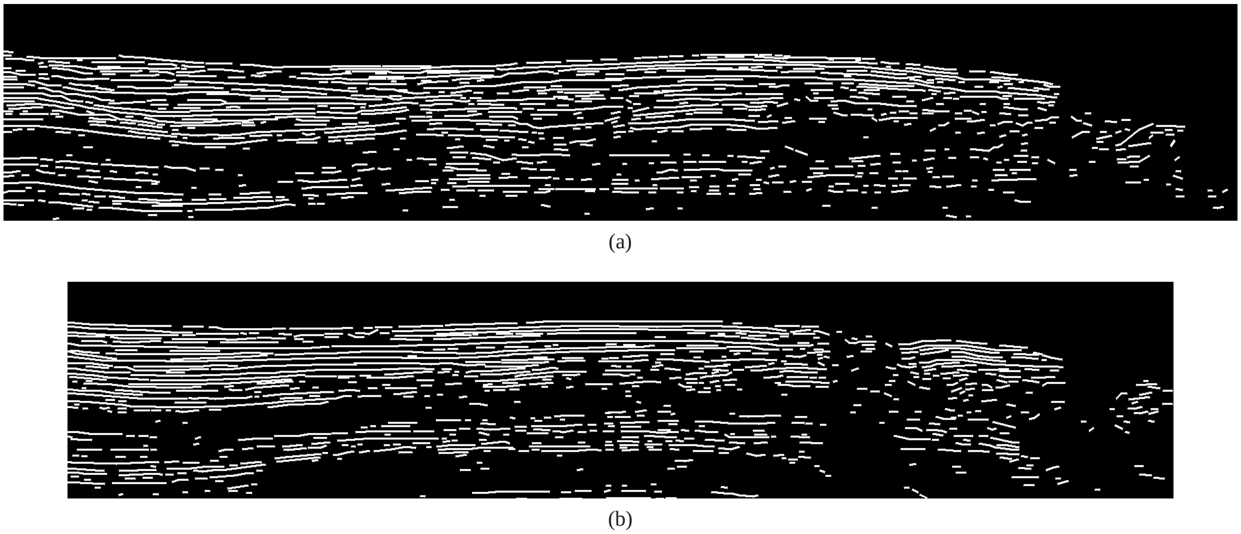

Fig. 10. Results obtained by the proposed technique on SHARAD radargrams (a) 520501000 and (b) 528401000 using $w = 2$ and $c_{\text{max}} = 3$.

linear features, and the background noise, depend on both the specific sounded area and the environmental conditions. The detection performance is assessed by measuring i) the number of correctly detected linear features and false alarms, and ii) the quality of the detections in terms of length of detected linear features versus their actual length. In order to measure such quantities we defined manually reference maps of the linear features present in the radargrams and compared them to the results of the proposed method. The reference maps do not contain lines shorter than 10 pixels in order to be comparable to the output of the proposed method.

1) Detection and False Alarm Rate: The number of lines present in the reference maps, the number of detected lines and the number of false alarms produced by the proposed technique are summarized in Tab. I for the four test radargrams. We consider a line detected if it overlaps with a line produced by the algorithm. Similarly, we consider a line produced by the algorithm as a false alarm if it does not overlap with any line contained in the reference map. The analysis of the results points out that the proposed technique has good performance, especially considering that it is automatic. In order to have a more detailed understanding of the detection rate of the method, we studied the relation between the number of missed, detected and false alarms and the line lengths. The results are reported in Fig. 11, which shows the histograms representing the number of detected (green), missed (red) and false (yellow) lines versus their length for the four test radargrams. The last column of the histograms includes the lines that have a length equal or greater than 195 pixels. The histograms show that the proposed method detected approximately all the linear features with a length greater than about 30 pixels. For shorter lines the detection performance decreases, and false alarms arise. This behavior is not an issue for the goal of the proposed technique, which is the automatic analysis of subsurface areas showing extended layering. It is expected that in such areas significant linear features have a long extension in the radargram domain.

2) Quality of Detection: In order to quantify the quality of the detection performed by the proposed method, we measured for each retrieved line the length of the detected part. This measure has been compared to the actual length of the line. Fig. 12 summarizes the results obtained on the four test radargrams. The figure shows for each test radargram a histogram representing the number of detected lines versus the ratio between detected length and actual length. The results point out that in most cases the algorithm is able to detect up to the 60-90% of the length of the linear features. A lower detection quality is associated with the radargram of Fig. 7d. This was expected, as the radargram shows less clear linear features with respect to the others.

TABLE I
ACCURACY PROVIDED BY THE PROPOSED TECHNIQUE FOR THE DETECTION OF LINEAR FEATURES IN RADAR SOUNDER DATA ON FOUR SHARAD RADARGRAMS.

Radargram number	**Number of lines**	**Detected lines**	**False alarms**
520501000	777	636	63
528401000	768	601	52
1041902000	694	591	78
1591701000	754	610	48

E. Extraction of Measurements of Interest

In Sec. III-D we defined several measurements that can be derived from the output of the linear feature detection. In this section we focus on the calculation of the number of detected lines and their density in a given radargram area. Indeed, such measurements are interesting as they can give a quick overview of the presence of subsurface linear features and of their distribution, and become important when 3D maps of these parameters should be obtained by interpreting radargrams acquired on parallel adjacent tracks in global mapping applications. Fig. 13 shows the measured number of lines per frame for the test radargrams of Fig. 7a and Fig. 7b. Both the number of layers present in the reference map and in the detected set are shown. The values have been averaged using a 10-wide moving window in order to reduce

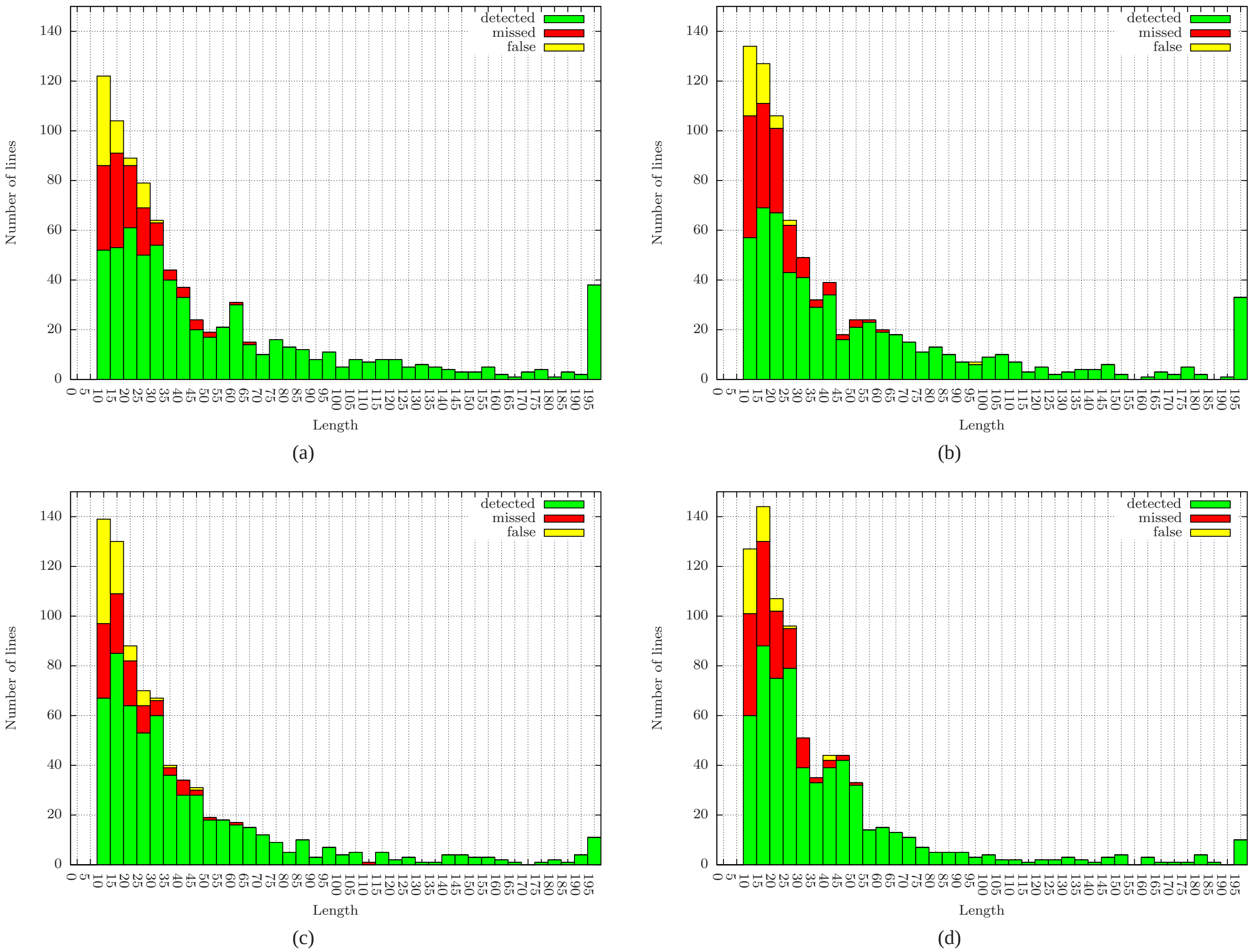

Fig. 11. Histograms representing the number of detected (green), missed (red) and false (yellow) lines versus their length for the four SHARAD test radargrams: (a) 520501000, (b) 528401000, (c) 1041902000, and (d) 1591701000.

the effect of outliers. The graphs show that the output of the proposed technique well approximates the values given by the reference maps. In general the proposed technique slightly underestimates the number of linear features. The largest gaps between the output of the algorithm and the reference map are due to low contrast linear features (low power at the interface) which are not detected.

Fig. 14 and Fig. 15 show the layer densities maps obtained for the same two test radargrams. Both the map obtained from the layer reference map and the detected map are shown for each radargram. The densities have been calculated using a sliding window of size 5×20 pixels (along-track $\times$ range) with a step of 1 pixel in both along-track and range directions. The measures obtained from overlapping windows have been averaged. The layer density is represented in terms of number of lines per samples. By considering the range sampling of the SHARAD radargrams (which is 37.5 ns), this means that the values shown in Fig. 14 and Fig. 15 correspond approximately to a range of 0 to 0.63 lines every 10 meters (using $\varepsilon_{\mathrm{SS}} = 3.15$). The choice of the size of the sliding window has been driven by the much different resolution of the data in the along-track and range direction. As commented in Sec. III-D5, the choice of a larger window would have produced smoothed versions of the density maps. The density maps of Fig. 14 and Fig. 15 present clearly how the linear features are distributed within the radargrams. A visual comparison between the reference density maps and the detected density maps shows that the proposed technique is able to approximate the reference map with good accuracy in a completely automatic way.

V. Conclusion

In this paper we presented a novel technique for the automatic detection and characterization of subsurface linear features in radar sounder data. The method is suited to the analysis of regions showing extended layering. The experimental results obtained on real planetary radar sounder data confirmed the effectiveness of the proposed method both qualitatively and quantitatively.

In order to extract further information from the radargrams, we also proposed a set of measurements which can be derived from the detected linear features. Such measures can describe locally the properties of the single linear features and provide

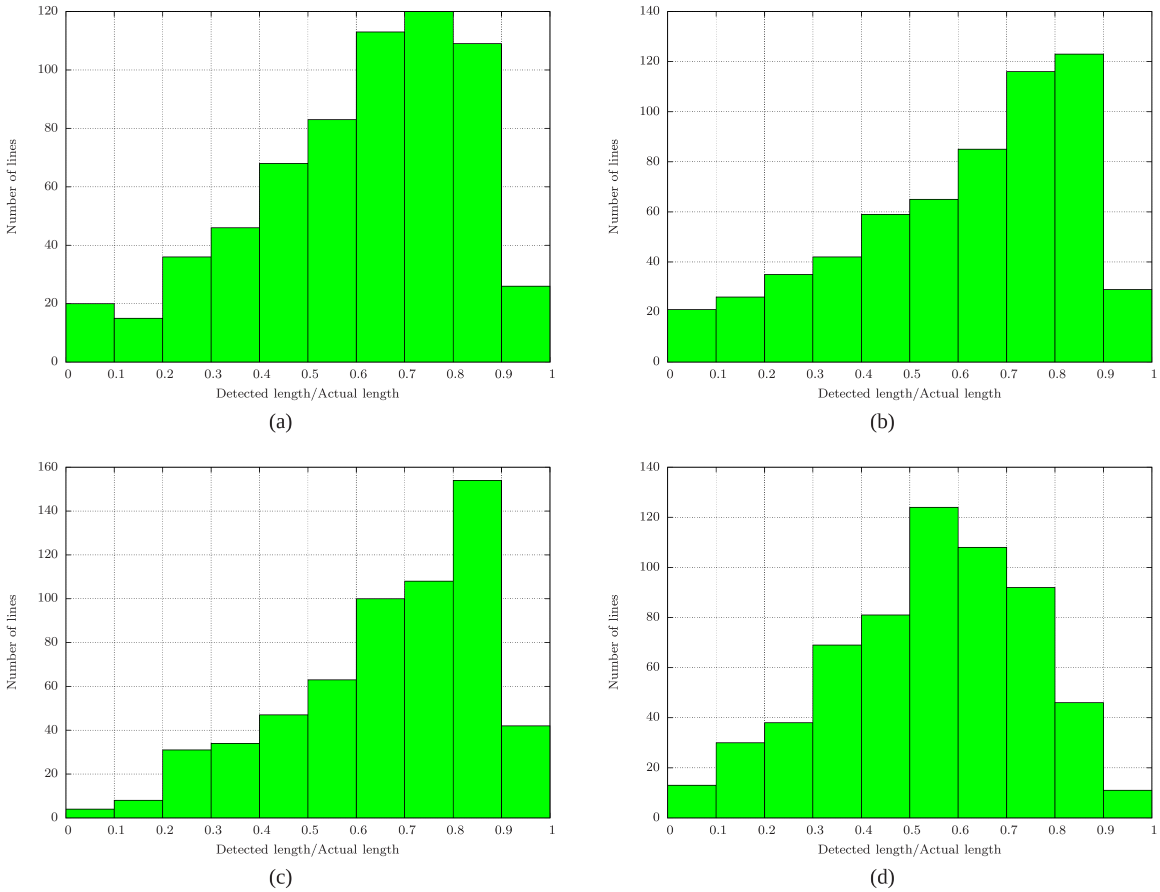

Fig. 12. Histograms representing the number of detected lines versus the ratio between their detected and actual lengths for the four SHARAD test radargrams: (a) 520501000, (b) 528401000, (c) 1041902000, and (d) 1591701000.

information about their distribution within the radargram (and thus the geographical area of interest).

The technique and the measurements proposed in this paper are relevant for the automatic analysis and combination of many radar sounder acquisitions over large areas. Indeed, they can provide in a fast way information on subsurface layering which can be used to derive high level products in a global mapping perspective, or to drive further manual analysis on interesting areas. At the present time, this is important especially for the analysis of the data provided by the currently operating radar sounders at Mars. However, the development of automatic methods such as the one proposed in this paper become important also for future spaceborne missions exploring other planetary bodies or the Earth's polar regions. In the latter case, it is expected that a radar sounder orbiting the Earth will provide a huge amount of high-precision data, allowing also multi-temporal studies. All these factors make automatic methods suitable for a fast and objective analysis of the data, which can help to provide information for the assessment of the impact of climate changes on the Earth's system.

As a final remark, we want to highlight that the research presented in this paper is a part of a more general framework aimed at the automatic extraction of information from radar sounder data. The future work related to the analysis of linear features will focus on the test of the proposed method on airborne datasets acquired at different frequencies and resolutions on the Earth's polar regions. Moreover, we plan to study automatic techniques for the automatic detection and filtering of linear features due to surface clutter from the output of the proposed technique.

Acknowledgment

The authors would like to thank Nathaniel E. Putzig from the Southwest Research Institute, Boulder, CO for providing information about the SHARAD data. We also acknowledge the Orfeo Toolbox (OTB) [35] and Insight Toolkit (ITK) [36] communities for publishing these libraries as open source products. This work has been supported by the Italian Space Agency (ASI).

References

[1] D. J. Daniels, *Ground penetrating radar (2nd Edition)*. London, UK: Institution of Engineering and Technology, 2007.

[2] D. Vaughan, H. Corr, F. Ferraccioli, N. Frearson, A. O'Hare, D. Mach, J. Holt, D. Blankenship, D. Morse, and D. Young, "New boundary conditions for the West Antarctic ice sheet: Subglacial topography beneath Pine Island Glacier," *Geophys. Res. Lett.*, vol. 33, p. L09501, 2006.

[3] IGOS, *Cryosphere Theme Report*. IGOS, 2007.

[4] T. Ono, A. Kumamoto, Y. Yamaguchi, A. Yamaji, T. Kobayashi, Y. Kasahara, and H. Oya, "Instrumentation and observation target of the Lunar Radar Sounder (LRS) experiment on-board the SELENE spacecraft," *Earth, Planets, and Space*, vol. 60, pp. 321–332, Apr. 2008.

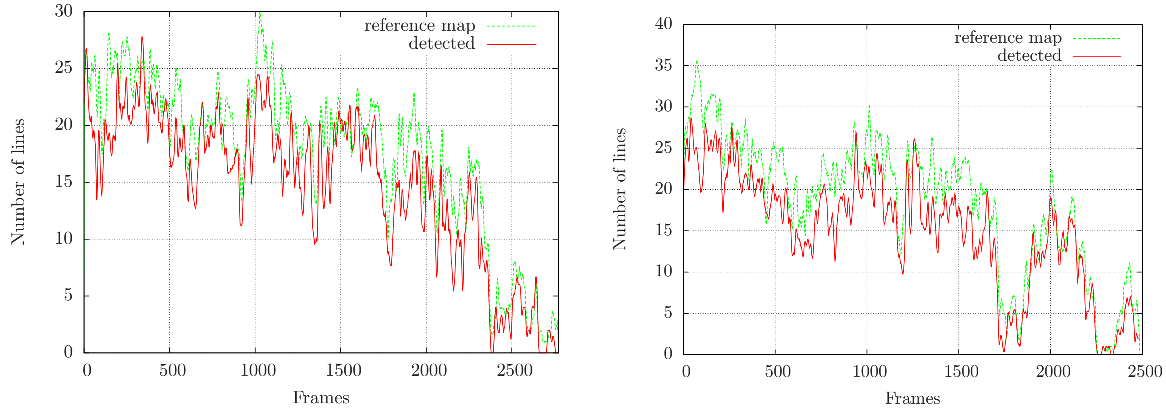

(a) (b)

Fig. 13. Number of detected lines per frame for the SHARAD test radargrams (a) 520501000, and (b) 528401000. The measured values have been averaged using a moving window of width equal to 10 frames.

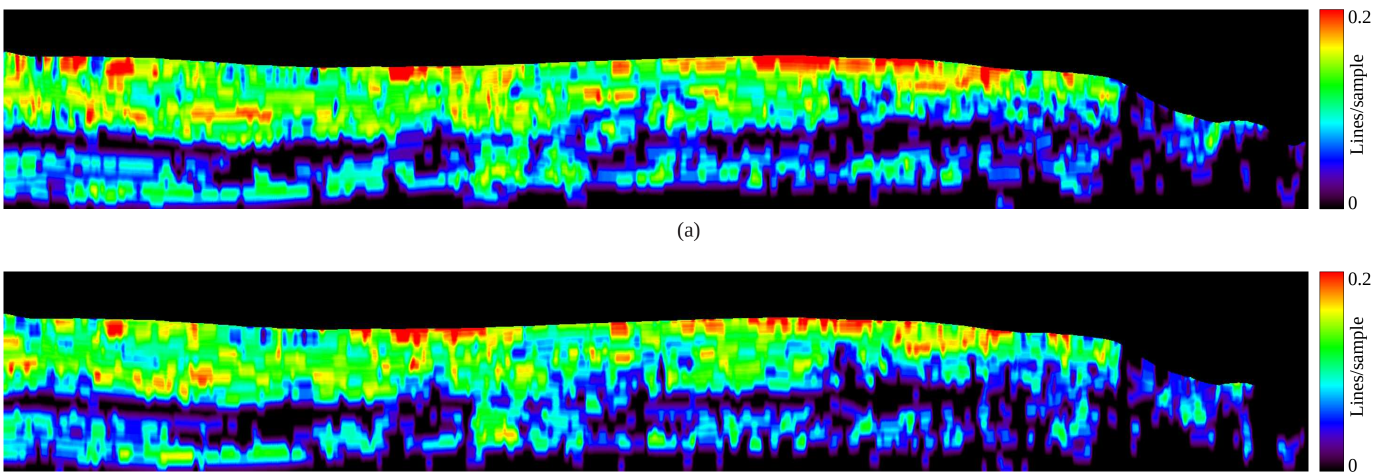

(a)

(b)

Fig. 14. Layer density measured using a sliding window of 5 × 20 pixels (along-track × range) with a step of 1 pixel in both along-track and range directions on (a) the reference map, and (b) the detected linear features of SHARAD radargram 520521000. The measured values have been averaged on overlapping windows.

[5] R. Jordan et al., "The Mars Express MARSIS sounder instrument," *Planetary and Space Science*, vol. 57, pp. 1975–1986, 2009.

[6] R. Seu et al., "SHARAD sounding radar on the Mars Reconnaissance Orbiter," *J. Geophys. Res.*, vol. 112, p. E05S05, 2007.

[7] J.J. Plaut et al., "Subsurface radar sounding of the South Polar Layered Deposits of Mars," *Science*, vol. 316, pp. 92–95, 2007.

[8] R. Seu et al., "Accumulation and erosion of Mars' South Polar Layered Deposits," *Science*, vol. 317, pp. 1715–1718, Sep. 2007.

[9] L. M. Carter et al., "Shallow radar (SHARAD) sounding observations of the Medusae Fossae Formation, Mars," *Icarus*, vol. 199, no. 2, pp. 295–302, Feb. 2009.

[10] L. Bruzzone, G. Alberti, C. Catallo, A. Ferro, W. Kofman, and R. Orosei, "Sub-surface radar sounding of the Jovian moon Ganymede," *Proc. IEEE*, vol. 99, no. 5, pp. 837–857, May 2011.

[11] "Titan Saturn System Mission NASA/ESA joint summary report," online: http://opfm.jpl.nasa.gov/library/, Jan. 2009.

[12] V. Bogorodsky, C. Bentley, and P. Gudmandsen, *Radioglaciology*. D. Reidel Publishing Co., 1985.

[13] D. Vaughan, H. Corr, C. Doake, and E. Waddington, "Distortion of isochronous layers in ice revealed by ground-penetrating radar," *Nature*, vol. 398, pp. 323–326, 1999.

[14] Waddington, E.D., et al., "Inference of accumulation-rate patterns from deep layers in glaciers and ice sheets," *J. of Glaciol.*, vol. 53, no. 183, pp. 694–712, 2003.

[15] A. Ferro and L. Bruzzone, "Analysis of radar sounder signals for the automatic detection and characterization of subsurface features," *IEEE Trans. Geosci. Remote Sens.*, in press 2012.

[16] L. Capineri, P. Grande, and J. A. G. Temple, "Advanced image-processing technique for real-time interpretation of ground-penetrating radar images," *International Journal of Imaging Systems and Technology*, vol. 9, no. 1, pp. 51–59, 1998.

[17] W. Al-Nuaimy, H. H. Lu, S. Shihab, and A. Eriksen, "Automatic mapping of linear structures in 3-dimensional space from ground-penetrating radar data," in *Remote Sensing and Data Fusion over Urban Areas, IEEE/ISPRS Joint Workshop 2001*, 2001, pp. 198 –201.

[18] E. Pasolli, F. Melgani, and M. Donelli, "Automatic analysis of GPR images: a pattern-recognition approach," *IEEE Trans. Geosci. Remote Sens.*, vol. 47, no. 7, pp. 2206–2217, Jul. 2009.

[19] P. Gamba and S. Lossani, "Neural detection of pipe signatures in ground penetrating radar images," *IEEE Trans. Geosci. Remote Sens.*, vol. 38, no. 2, pp. 790 –797, Mar. 2000.

[20] S. Delbo, P. Gamba, and D. Roccato, "A fuzzy shell clustering approach to recognize hyperbolic signatures in subsurface radar images," *IEEE Trans. Geosci. Remote Sens.*, vol. 38, no. 3, pp. 1447 –1451, May 2000.

[21] G. J. Freeman, A. C. Bovik, and J. W. Holt, "Automated detection of near surface martian ice layers in orbital radar data," in *Image Analysis Interpretation (SSIAI), 2010 IEEE Southwest Symposium on*, may 2010, pp. 117 –120.

[22] K. Dabov, A. Foi, V. Katkovnik, and K. Egiazarian, "Image denoising by sparse 3D transform-domain collaborative filtering," *IEEE Trans. Image Process.*, vol. 16, no. 8, pp. 2080–2095, Aug. 2007.

[23] S. Parrilli, M. Poderico, C. Angelino, G. Scarpa, and L. Verdoliva, "A nonlocal approach for SAR image denoising," in *IEEE International Geoscience and Remote Sensing Symposium (IGARSS)*, 25-30 July,

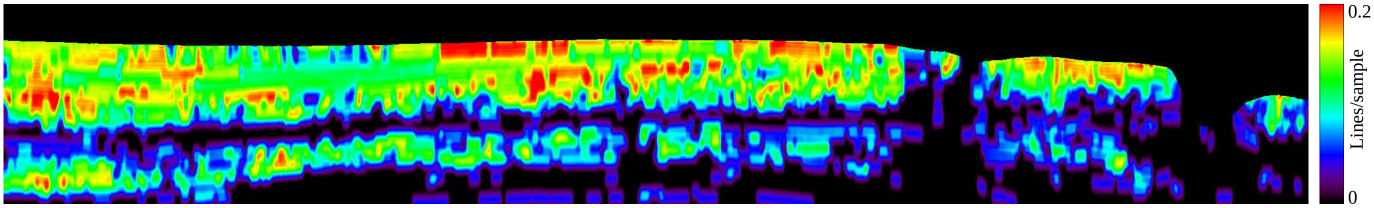

(a)

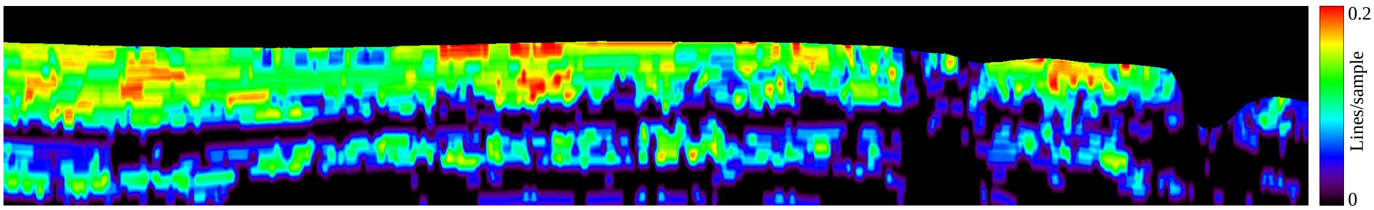

(b)

Fig. 15. Layer density measured using a sliding window of 5 $\times$ 20 pixels (along-track $\times$ range) with a step of 1 pixel in both along-track and range directions on (a) the reference map, and (b) the detected linear features of SHARAD radargram 528421000. The measured values have been averaged on overlapping windows.

Honolulu, HI, USA, 2010, pp. 726–729.

[24] M. Mäkitalo, A. Foi, D. Fevralev, and V. Lukin, "Denoising of single-look SAR images based on variance stabilization and nonlocal filters," in *International Conference on Mathematical Methods in Electromagnetic Theory (MMET)*, Sep. 2010, pp. 1–4.

[25] C. Oliver and S. Quegan, *Understanding Synthetic Aperture Radar Images*. Raleigh, NC, USA: SciTech Publishing, Inc., 2004.

[26] K. Dabov, A. Foi, V. Katkovnik, and K. Egiazarian, "Joint image sharpening and denoising by 3D transform-domain collaborative filtering," in *Int. TICSP Workshop Spectral Meth. Multirate Signal Process. (SMMSP)*, Sep. 2007.

[27] C. Steger, "An unbiased detector of curvilinear structures," *IEEE Trans. Pattern Anal. Mach. Intell.*, vol. 20, no. 2, pp. 113–125, Feb. 1998.

[28] ——, "Evaluation of subpixel line and edge detection precision and accuracy," in *International Archives of Photogrammetry and Remote Sensing*, 1998, pp. 256–264.

[29] A. Thiele, E. Cadario, K. Schulz, U. Thoennessen, and U. Soergel, "Building recognition from multi-aspect high-resolution InSAR data in urban areas," *IEEE Trans. Geosci. Remote Sens.*, vol. 45, no. 11, pp. 3583–3593, Nov. 2007.

[30] A. Ferro, D. Brunner, and L. Bruzzone, "Building detection and radar footprint reconstruction from single VHR SAR images," in *IEEE International Geoscience and Remote Sensing Symposium (IGARSS)*, 25-30 July, Honolulu, HI, USA, 2010.

[31] J. W. Holt, M. E. Peters, S. D. Kempf, D. L. Morse, and D. D. Blankenship, "Echo source discrimination in single-pass airborne radar sounding data from the Dry Valleys, Antarctica: Implications for orbital sounding of Mars," *J. Geophys. Res.*, vol. 111, p. E06S24, 2006.

[32] A. Ferro and L. Bruzzone, "A novel method for automatic clutter detection in radargrams acquired by orbiting radar sounders," in *IEEE International Geoscience and Remote Sensing Symposium (IGARSS)*, accepted, 2012.

[33] M. Zuber, D. Smith, S. Solomon, D. Muhleman, J. Head, J. Garvin, J. Abshire, and J. Bufton, "The Mars Observer Laser Altimeter investigation," *J. Geophys. Res.*, vol. 97, no. E5, pp. 7781–7797, 1992.

[34] B. A. Campbell, N. E. Putzig, L. M. Carter, and R. J. Phillips, "Autofocus correction of phase distortion effects on SHARAD echoes," *IEEE Geosci. Remote Sens. Lett.*, vol. in press, 2011.

[35] J. Inglada and E. Christophe, "The Orfeo Toolbox remote sensing image processing software," in *IEEE International Geoscience and Remote Sensing Symposium (IGARSS)*, 2009.

[36] L. Ibanez, W. Schroeder, L. Ng, J. Cates, Consortium T.I.S., and R. Hamming, *The ITK Software Guide*. Kitware, Inc., 2003.

Adamo Ferro received the M.S. degree in telecommunications engineering (summa cum laude) and the Ph.D. degree in telecommunications from the University of Trento, Trento, Italy, in 2008 and 2011, respectively.

During summer 2010, he was a visiting Ph.D. student at the Jet Propulsion Laboratory, California Institute of Technology/NASA, Pasadena. He is currently with the Remote Sensing Laboratory in the Department of Information Engineering and Computer Science, University of Trento. His main interests include the analysis of planetary radar sounder signals for information extraction purposes, and very high resolution synthetic aperture radar signal characterization in urban environments aimed at the automatic extraction of man-made structures. He is Participating Scientist of the Shallow Radar (SHARAD) instrument science team.

Dr. Ferro was a recipient of the prize for the best Italian Master Thesis on Remote Sensing presented in 2008 awarded by the IEEE Geoscience and Remote Sensing South Italy Chapter.

Lorenzo Bruzzone (S'95-M'98-SM'03-F'10) received the laurea (M.S.) degree in electronic engineering (summa cum laude) and the Ph.D. degree in telecommunications from the University of Genoa, Italy, in 1993 and 1998, respectively. He is currently a Full Professor of telecommunications at the University of Trento, Italy, where he teaches remote sensing, radar, pattern recognition, and electrical communications. Dr. Bruzzone is the founder and the director of the Remote Sensing Laboratory in the Department of Information Engineering and Computer Science, University of Trento. His current research interests are in the areas of remote sensing, radar and SAR, signal processing, and pattern recognition. He promotes and supervises research on these topics within the frameworks of more than 28 national and international projects. He is the author (or coauthor) of 114 scientific publications in referred international journals (76 in IEEE journals), more than 170 papers in conference proceedings, and 16 book chapters. He is editor/co-editor of 10 books/conference proceedings and 1 scientific book. He has served on the Scientific Committees of several international conferences and was invited as keynote speaker in more than 20 international conferences and workshops. He is a member of the Managing Committee of the Italian Inter-University Consortium on Telecommunications. Since 2009 he is a member of the Administrative Committee of the IEEE Geoscience and Remote Sensing Society. Dr. Bruzzone ranked first place in the Student Prize Paper Competition of the 1998 IEEE International Geoscience and Remote Sensing Symposium (Seattle, July 1998). He was a recipient of the Recognition of IEEE Transactions on Geoscience and Remote Sensing (TGRS) Best Reviewers in 1999 and was a Guest Co-Editor of different Special Issues of international journals. In the past years joint papers presented by his students at international symposia and master theses that he supervised have received international and national awards. He was the General Chair/Co-chair of the First, Second and Sixth IEEE International Workshop on the Analysis of Multi-temporal Remote-Sensing Images (MultiTemp), and is currently a member of the Permanent Steering Committee of this series of workshops. Since 2003, he has been the Chair of the SPIE Conference on Image and Signal Processing for Remote Sensing. From 2004 to 2006 he served as an Associated Editor of the IEEE Geoscience and Remote Sensing Letters, and currently is an Associate Editor for the IEEE TGRS and the Canadian Journal of Remote Sensing. Since April 2010 he has been the Editor of the IEEE Geoscience and Remote Sensing Newsletter. In 2008 he has been appointed as a member of the joint NASA/ESA Science Definition Team for the radar instruments for *Outer Planet Flagship Missions*. Since 2012 he has been appointed *Distinguished Speaker* of the *IEEE Geoscience and Remote Sensing Society*. Dr. Bruzzone is member of the Italian Association for Remote Sensing (AIT).